Stability Analysis of Power Systems With Multiple STATCOMs in Close Proximity

Chi Li, *Member, IEEE*, Rolando Burgos, *Member, IEEE*, Bo Wen, *Member, IEEE*, Ye Tang, *Student Member, IEEE*, and Dushan Boroyevich, *Life Fellow, IEEE*

***Abstract*—Recently, multiple static synchronous compensator (STATCOM) units have been adopted in power transmission systems in order to obtain a better voltage regulation and to share loads. However, they could possibly interact in a negative way instead of helping each other, due to the improper design of the STATCOM controllers. To analyze this problem, a *d–q* frame impedance-based stability analysis was used to explore the instability with the presence of STATCOMs, where previous stability-related findings are not applicable directly because of some unique features of STATCOMs. This paper identified the frequency range of interactions in a viewpoint of *d–q* frame impedances and pinpointed that the ac voltage regulation was the main reason of instability, masking the effects of phase-locked loop on power transmission systems. In addition, due to the high impedance of STATCOMs around the frequency range of interactions, the number of connected STATCOMs was the main contributor to stability instead of the topology of power systems or the locations of STATCOMs. A scaled-down 2-STATCOM power grid was built to verify the conclusions experimentally. This paper is accompanied by a video showing instability between STATCOMs in the experiment.**

***Index Terms*—Impedance-based stability criterion, small-signal impedance, stability, static synchronous compensators (STATCOM).**

I. Introduction

STATIC synchronous compensators (STATCOMs) have been widely adopted in modern power systems to offer reactive power compensation [1], [2] and enhance stability performances [3]–[5]. It is a common practice to install a STATCOM at the bus either where it can regulate the bus voltages over the grid to its best performance, or where some renewable energy is connected. However, this single-STATCOM approach may not be the best solution in every power system because of the following reasons. First of all, reactive power cannot be delivered through long distances, and a single STATCOM may not be able to maintain all the bus voltages [6], [7]. Second, more than one STATCOM can possibly achieve better oscillation damping [8], [9]. Third, several STATCOMs that are small in power rating could be more economic than a large one. Due to the aforementioned considerations, there is a power transmission grid from Dominion Energy with four STATCOMs installed in physical proximity, about 10 miles away [10].

By having multiple STATCOMs installed adjacently, a better voltage profile over the grid can be obtained, and the STATCOMs are able to share the load burden. Additionally, flexibility of an operation is available to facilitate maintenance, and, for example, one STATCOM can be disconnected from the grid for the maintenance or adjustment while the others are online. However, during the deployment of such facility with multiple STATCOMs, a huge effort is necessary on tuning controllers of the STATCOMs to ensure power system stability when they are working together. Researchers have been studying the influences of a single STATCOM connected to a given power grid, including steady state, small-signal, and large-signal stability. STATCOMs can induce instability to a power system due to interactions with other power electronic converters in the system, such as a high-voltage direct current (HVdc) transmission station [11]–[14], or a wind farm [15]–[20]. However, instability due to interactions between STATCOMs is not yet documented, except our preliminary results presented in [11]. The existing discussions on multiple STATCOMs are mostly focused on steady-state analysis, for example, allocation and sizing [12]–[15] and coordinated secondary voltage regulation [6], [7], [9], [16]–[18]. This paper will try to fill the blanks in small-signal stability, starting from assessments of a power system with multiple STATCOMs in proximity to see how multiple STATCOMs could interact and what the crucial reason of the potential instability is.

In this paper, the targeted scenario is that each STATCOM is individually designed to be the best, without knowing the existence of the other ones. This scenario is likely to happen when the STATCOMs are from different vendors and there is very limited information flowing between the vendors to achieve globally optimized design for all the STATCOMs. Admittedly, if one could access the full information, i.e., the power system parameters and all the STATCOM parameters, it is possible to optimize the STATCOM parameters to guarantee stability. However, this ideal condition would be unattainable in many practical cases. Therefore, the selection and optimization of the STATCOM control parameters are based on each STATCOM's

Manuscript received January 25, 2018; revised May 22, 2019; accepted July 15, 2019. Date of publication July 29, 2019; date of current version December 13, 2019. This work was supported by Dominion Energy through its Fellowship Program at the Center for Power Electronics Systems (CPES), as well as by the Wide Bandgap High Power Converters and Systems mini-consortium at CPES. Recommended for publication by Associate Editor B. Singh. *(Corresponding author: Chi Li.)*

C. Li is with the Department of Electrical Engineering, Tsinghua University, Beijing 100084, China (e-mail: lichi@tsinghua.edu.cn).

R. Burgos, B. Wen, Y. Tang, and D. Boroyevich are with the Bradley Department of Electrical and Computer Engineering, Virginia Tech, Blacksburg, VA 24061 USA (e-mail: rolando@vt.edu; wenbo@vt.edu; yetang@vt.edu; dushan@vt.edu).

This paper has supplementary downloadable multimedia material available at http://ieeexplore.ieee.org, provided by the authors.

Color versions of one or more of the figures in this paper are available online at http://ieeexplore.ieee.org.

Digital Object Identifier 10.1109/TPEL.2019.2931891

terminal and the corresponding Thevenin equivalent circuit of the power system, assuming that the buses of the other STATCOMs were ideal PV or PQ buses, or with detailed state-space models if available. The parameter optimization is designed by control loop gains, which is a typical design approach for power electronics converters and how STATCOM vendors would do in practice. Usually, the vendors will be offered with a simplified system network from the system operator or integrator, and the design will be based on that. When installing the real equipment, engineers from the STATCOM vendors would tune the control parameters on field.

There are many methods to study small-signal stability in power systems, for example, state-space-model-based method [19], impedance-based method, and phasor-based method [20]. Using the state-space model, a full-order model of a STATCOM, including the details of the controller, was presented in [21]. Impedance-based stability analysis, which has been proven of great success in dc systems for a long time [22] and has since then become attractive too in power-electronics-based three-phase ac systems [23]–[33]. Such analysis uses the measurable terminal characteristics of power converters, that is, their small-signal input and output impedances, to analyze the small-signal stability at a given ac bus or interface at a given operating point. As such, this approach can assess the small-signal stability of systems without knowing the internal details of power converters and other power system components, representing a significant advantage for system integrators. Specifically, constant power load (CPL) dynamics were found to trigger instability in three-phase power electronics systems [23], [25], [27], where the d-channel impedance element was the main reason of instability. On the other hand, synchronization to the grid with inverters injecting active power was identified to be another source of instability [29], where the instability was found as a result of interactions of impedances in the q-channel.

However, several key features of STATCOMs distinguish themselves from the existing research, which ultimately determine different possibilities of a STATCOM to induce dynamic interactions with other system components. The first one is that the impedance of a STATCOM, working at nearly zero power factor, has strong coupling between its d–q channels, which renders all *d–q* frame impedance elements of similar magnitude. In the unity power factor case as in previous research [23], [27], [29], the magnitude of Z_{dd} and Z_{qq} elements are much larger than the cross-coupling terms Z_{dq} and Z_{qd}, which under specific circumstances can simplify the assessment of stability by avoiding the use of a multivariable stability theory, such as the generalized Nyquist criterion (GNC), allowing for the use of the standard Nyquist criterion across the single-input single-output d–d and q–q channels directly. However, in the STATCOM case, the similar magnitude of all impedance elements makes the stability assessment a multivariable problem requiring the use of the GNC to determine the small-signal stability at a given ac interface. As such, the eigenvalues of the return ratio matrix, which is the product of the upstream and downstream impedances seen at the ac interface, need be examined by applying the GNC, as the analysis of the *d–q* frame impedances will be inconclusive. The second feature is that the negative-incremental input impedance of a STATCOM can be reflected either on its *d*- or *q*-axis channel depending on its reactive power operating mode, where reactive power is generated to support the grid voltage and absorbed under high-voltage conditions [30]. This unique characteristic represents a challenge from a stability standpoint, as previous findings had shown that instability could be triggered either in the d-channel due to CPL dynamics [27], or in the q-channel as a result of active power being injected synchronously into the grid [29]. STATCOMs, with their dual behavior, and hence double challenge, embody in consequence a new instability pattern in power system. The third feature is that STATCOMs, by nature, compensate the voltage at the point of common coupling (PCC), which is also where they synchronize their operation. As a result, their synchronization and ac voltage compensation loops are inherently and strongly coupled from a control standpoint, as they do not simply track the grid voltages, but regulate them. All these dynamic characteristics differ significantly from those of grid-tied inverters and rectifiers, which renders previous stability-related findings for these converters nonapplicable directly. This paper will aim to address these issues and discover the roots of potential instability.

The rest of this paper is organized as follows. Section II presents the IEEE 14-bus system with four STATCOMs with their control; Section III shows the potential instability due to STATCOM control; Section IV uses *d–q* frame impedances to analyze the instability phenomena; Section V shows experimental verification with a scaled-down 2-STATCOM prototype system; and Section VI concludes this paper.

II. IEEE 14-Bus System With Four STATCOMs

To generalize the analysis on interactions between STATCOMs, an IEEE 14-bus system test bed was selected with four STATCOMs placed nearby, as shown in Fig. 1. The four STATCOMs are installed at different buses in the 230-kV transmission grid, as shown in Fig. 1, where each thin line represents a transmission line with its impedance.

The topology of the STATCOM under consideration, shown in Fig. 2, was assumed as a two-level converter and a step-up transformer, which is reasonable in terms of power-system-level dynamics and control. More recently, modular multilevel converter (MMC)-type STATCOMs have been introduced, which, however, feature similar dynamics from synchronization, current loop, and voltage regulation loops, that is, in their low-frequency range characteristics. The main results herein presented can then be generalized, from an ac-terminal standpoint to other multilevel and MMC-type topologies. The control system of the STATCOM in question, as shown in Fig. 2, features an inner current-loop and outer voltage-loop, both of them oriented by a phase-locked loop (PLL) tracking the PCC voltage. The inner current-loop is decoupled in the *d–q* frame prior to generating the duty cycles (d) for the PWM block that generates the gating signals to drive the semiconductor devices. In the current loop, the d-channel is used to regulate the dc bus voltage and the q-channel to regulate the ac-bus voltage magnitude. An optional reactive power–voltage (QV) droop curve uses the actual reactive power output to modify the PCC voltage reference.

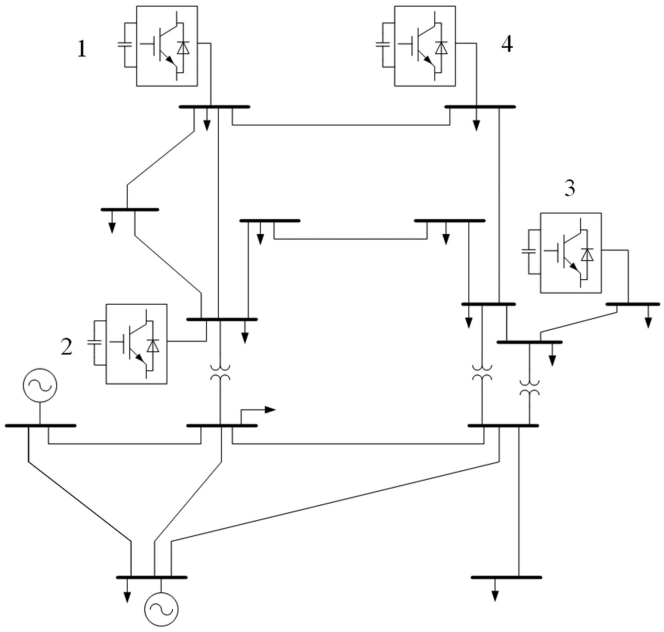

Fig. 1. IEEE 14-bus system with four STATCOMs.

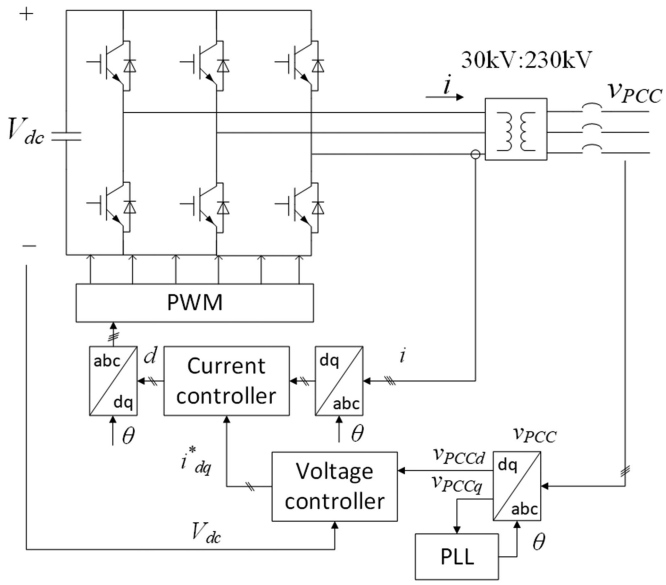

Fig. 2. Schematics of a STATCOM with its controller.

Fig. 3 shows the details, where variables with an asterisk $(*)$ corresponds to reference signals; subscript d means variables in the d-channel, and subscript q means variables in the q-channel. The inner current-loop is controlled in the d–q frame, where the d-channel compensator is G_{cid} and the q-channel compensator is G_{ciq}. The d-channel current reference is provided to maintain the dc bus voltage using dc voltage compensator $G_{cv\mathrm{dc}}$, and the q-channel current reference is given to regulate the ac bus voltage magnitude via the ac bus voltage compensator $G_{cv\mathrm{ac}}$. Outside the ac voltage loop, there is an optional QV droop to allow the PCC voltage vary in an acceptable range in order to lessen the burden of the STATCOM. This additional loop is shown in

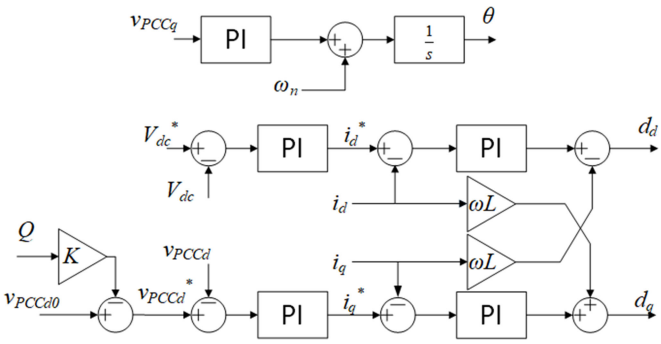

Fig. 3. Details of STATCOM control.

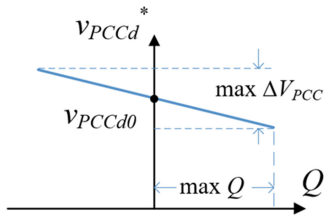

Fig. 4. QV droop for STATCOM control.

Fig. 4, where K represents the slope and $v_{\mathrm{PCC}d0}$ is the set point when the STATCOM generates zero reactive power. The PLL is a synchronous reference frame PLL that regulates the q-channel ac bus voltage to be zero using the PLL compensator $G_{c\mathrm{PLL}}$ to track the grid voltage

$$K = \frac{\max \Delta V_{\mathrm{PCC}}}{2\,|\max Q|}. \tag{1}$$

A simple design procedure for the compensators is followed per [34]

$$G_{cid} = G_{ciq} = k_{pi} + \frac{k_{ii}}{s}, \text{where } k_{pi} = \frac{\omega_{ci} L}{V_{dc}}, k_{ii} = \frac{\omega_{ci} R}{V_{\mathrm{dc}}} \tag{2}$$

$$G_{cvac} = k_{pvac} + \frac{k_{ivac}}{s}, \text{where } k_{pvac} = \frac{\omega_{cv}}{\omega_{ci}\omega_n L_g},$$

$$k_{ivac} = \frac{\omega_{cv}}{\omega_n L_g} \tag{3}$$

$$G_{c\mathrm{PLL}} = k_{p\mathrm{PLL}} + \frac{k_{i\mathrm{PLL}}}{s}, \text{where } k_{p\mathrm{PLL}} = \frac{\omega_{c\mathrm{PLL}}}{V_{\mathrm{PCC}d}}, k_{i\mathrm{PLL}} = 0 \tag{4}$$

where ω_{ci} is the bandwidth of current loop, ω_{cv} is the bandwidth of ac voltage loop, $\omega_{c\mathrm{PLL}}$ is the bandwidth of PLL, L is the transformer inductor, R is the parasitic resistor, V_{dc} is the dc bus voltage, ω_n is the line frequency, L_g is the Thevenin grid inductor, and $V_{\mathrm{pcc}d}$ is the d-channel grid voltage at PCC. The controllers were designed based on the Thevenin equivalent grid impedance L_g at their terminal as a benchmark individually. The PLL was designed with 5 Hz bandwidth and 85° phase margin for 60 Hz grid frequency to attenuate detected frequency. A current loop with 200 Hz bandwidth and 90° phase margin, assuming

TABLE I
PARAMETERS OF STATCOMs

Parameter	Symbol	Value
DC bus voltage	V_{dc}	100 kV
D-channel PCC bus voltage in system d-q frame	V^s_{PCCd}	30.35 kV
Q-channel PCC bus voltage in system d-q frame	V^s_{PCCq}	-465.2 V
D-channel grid side current in system d-q frame	I^s_d	-9.12 A
Q-channel grid side current in system d-q frame	I^s_q	-1.78 kA
Inductance of step-up transformer	L	7.3 mH
Resistance of step-up transformer	R	21 mΩ
Capacitance of the dc capacitor	C_{dc}	100 mF
Discharging resistor in dc side	R_{dc}	20 kΩ
Current controller $k_{pi} + k_{ii}/s$	k_{pi}	0.00017
	k_{ii}	0.015
Current loop bandwidth	f_{ci}	200 Hz
PLL controller $k_{pPLL} + k_{iPLL}/s$	k_{pPLL}	0.002
	k_{iPLL}	0.02
PLL bandwidth	f_{cPLL}	5 Hz
AC voltage controller $k_{pac} + k_{iac}/s$	k_{pac}	0.445
	k_{iac}	222.5
AC voltage loop bandwidth	f_{cvac}	7 Hz
DC voltage controller $k_{pdc} + k_{idc}/s$	k_{pdc}	1.25
	k_{idc}	0.225
DC voltage loop bandwidth	f_{cvdc}	0.1 Hz

the equivalent switching frequency to be 2 kHz, was designed to ensure a good current waveform. The ac voltage loop was tuned to be at 7 Hz bandwidth with 45° phase margin, and the dc voltage loop was adjusted to be at 0.1 Hz bandwidth with 60° phase margin. Every STATCOM was stable by itself connecting to the power system with enough phase margins. The parameters of studied STATCOMs are shown in Table I in simulation, and the four STATCOMs are identical. Note that all the variables are transformed to the low-voltage side of the transformer.

III. Potential Instability Due to STATCOM Control

In this section, the STATCOM was modeled in time domain using state-space averaging equations. The model can be found in Appendix A to save space as this is not the focus of this paper. With that, the evaluation was done in time-domain simulation in MATLAB/Simulink because it also provides plentiful functions in frequency-domain analysis. The four STATCOMs were successively connected online at the moments of 1, 3, 5, and 7 s, as shown in the marked order in Fig. 1. The effects of the ac voltage loop, the PLL, and the QV droop were assessed with the d-channel voltage at the terminal of STATCOM 1, shown as an indicator of stability. For each control loop, the system was evaluated with two different control bandwidths. Under any case with different control bandwidths, STATCOMs could work individually with sufficient phase margins but they could interact with each other in a negative way. In the following figures, stable cases are plotted in blue, and unstable cases are plotted in orange.

Fig. 5 depicts how the system would behave with two ac voltage loop bandwidths: When its bandwidth was 7 Hz (blue), the system was stable with four STATCOMs connected; when the bandwidth was increased to 16 Hz (orange), the system had faster responses before the fourth STATCOM working and

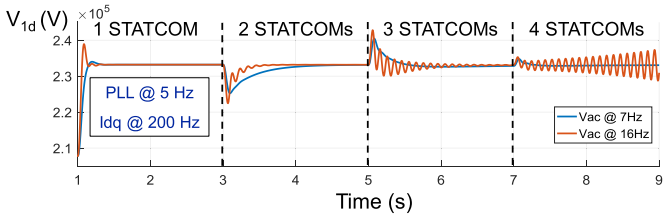

Fig. 5. Potential instability due to ac voltage loop.

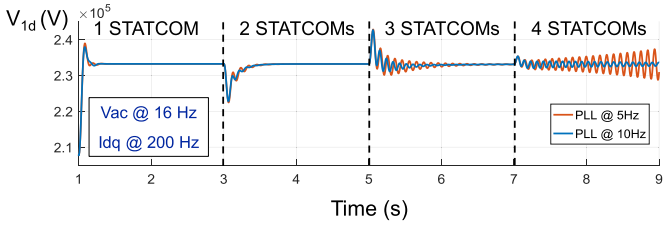

Fig. 6. Potential instability due to PLL.

unstable when the fourth connected at the oscillatory frequency of about 10 Hz. Note that at this time the QV droop was not functioning. With increasing ac voltage loop bandwidth, the system tended to be more unstable. Actually, the connection sequence of the STATCOMs did not matter in terms of stability, no matter which STATCOM was connected first or last, and this held for all the cases. This is because in the frequency range of instability, the STATCOM dynamics were dominant in frequency responses, which will be further analyzed from impedance point of view in Section IV-D.

The effects of the PLL bandwidth are shown in Fig. 6. Still, the QV droop was not running at this time. When the PLL bandwidth was low, i.e., 5 Hz (plotted by orange color in Fig. 6), the system was unstable; when the PLL bandwidth was increased to 10 Hz (plotted by blue in Fig. 6), the system became damped and stable. A higher PLL bandwidth tended to stabilize the system.

The above-mentioned two assessments showed that the ac voltage loop and PLL posed influences on stability. However, STATCOMs are trying to compensate the voltage at the PCC, where they are synchronized, and, thus, synchronization and ac voltage compensation are naturally coupled in control. When instability happened in the presence of STATCOMs [32], [33], it is necessary to point out what was the root of instability and to identify which control loop had the most influence in order to distinguish impedance behaviors from different control loops. Usually for a 50- or 60-Hz power grid, it is reasonable to tune the PLL bandwidth to be several Hertz, to suppress harmonics in synchronization. On the other hand, grid codes often require STATCOMs to compensate voltage fluctuations within a few line periods, and it means that the ac voltage loop bandwidth should be about 10 Hz. As such, it is difficult to differentiate dynamic responses from the ac voltage loop and the PLL because they have similar bandwidths. Their coupled effects on stability will be elaborated from impedance point of view in the following section and also the origin of instability will be pinpointed.

Fig. 7 presents how the QV droop influenced the system stability. The ac voltage loop bandwidth was tuned to 14 Hz to

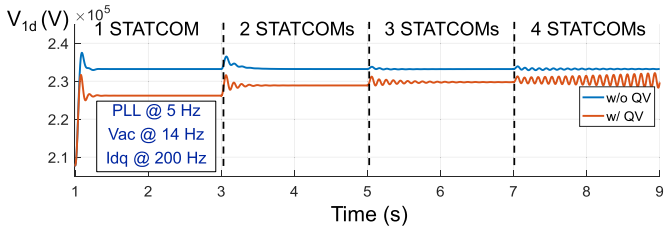

Fig. 7. Potential instability due to QV droop.

make the system stable with four STATCOMs running without the QV droop activation, and the waveform is plotted in blue. The waveform in orange shows the case with the QV droop. Clearly, the PCC voltage was smaller in magnitude, thanks to the QV droop which allowed the voltage to be within a certain range instead of a fixed value in order to lessen the output reactive power burden. However, with the QV droop when the fourth STATCOM was connected, the systems was unstable. The QV droop strengthened the interactions between STATCOMs and there were higher possibility that they could behave in an undesired manner. Actually, no QV droop is equavalent to zero droop coefficient with the QV droop. Thus, deactivation of the QV droop or a small droop coefficient was preferred in terms of stability.

IV. Impedance-Based Stability Analysis

In order to analyze the previously found instability phenomena, *d–q* frame impedance was used in this section. Separated at the PCC of STATCOM 1, impedances from both sides, called $\mathbf{Z_{vsi}}(s)$ for STATCOM impedance and $\mathbf{Z_{grid}}(s)$ for the rest of the grid including the other three STATCOMs, were measured in Simulink at the moment of7 s when the fourth STATCOM was just connected. There are two ways to obtain the impedances and both can provide accurate results. One is to linearize the whole system at this moment, which can only be done in the system modeled in the *d–q* frame where dc operating points exist. This method is easier but only available in simulation, with which the impedance results presented in Section IV were obtained. The other way is practical in use and applies to experiments also, which was used in Section V. For the second approach, an impedance measurement unit is required, which essentially sends out perturbations to the system under test, measures the responses, and calculates impedances. For stable cases, impedance measurements are done only once, as it is possible to obtain impedances from both sides at the same time. For unstable cases, impedance measurements are done twice, one impedance at one time to ensure a stable operation during measurements. It is accomplished by adjusting the control parameters of units that are not under test, meanwhile making sure that the operating point does not differ from the cases of interest.

Using GNC [23], one can examine the system stability by examining the eigenvalues of the return ratio $\mathbf{L}(s) = \mathbf{Z_{grid}}(s)\mathbf{Z_{vsi}}(s)^{-1}$. The system will be stable if and only if the net sum of anticlockwise encirclements of the critical point $(-1+\text{j}0)$ by the set of characteristic loci of $\mathbf{L}(s)$ is equal to the total number of right half plane (RHP) poles of $\mathbf{Z_{grid}}(s)$ and $\mathbf{Z_{vsi}}(s)^{-1}$. Additionally, one would be able to evaluate the stable regions by examining the characteristic loci. More conservatively, sufficient conditions for system stability were presented through different norms of the impedances, as in [23] and [35].

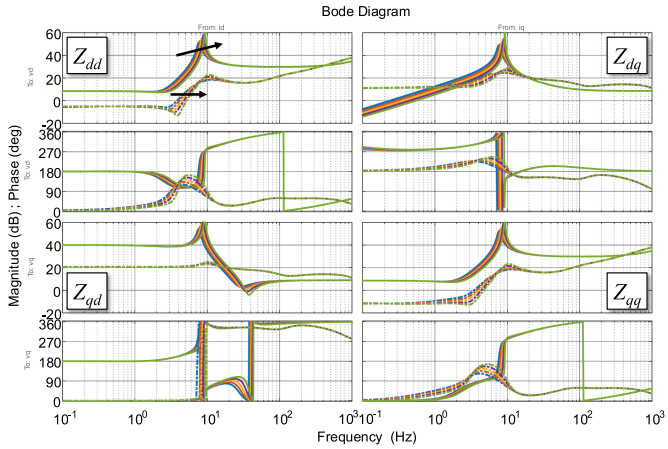

Fig. 8. Impedances at STATCOM 1 terminal with respect to ac voltage loop: solid line—Z_{vsi}; dashed line—Z_{grid}.

From our previous work on impedance modeling of STATCOMs [36], the impedance model is

$$\mathbf{Z_{vsi}} = \left\{ \begin{bmatrix} \mathbf{Y_{ol}} + \mathbf{G_{id}}(\mathbf{T} + \mathbf{G_{ci}}\mathbf{G_{cvdc}}\mathbf{G_{vdcd}})^{-1} \\ \mathbf{T}\mathbf{G}^{\mathbf{d}}_{\mathbf{PLL}} - \mathbf{G_{ci}} \left(\begin{matrix} \mathbf{G}^{\mathbf{i}}_{\mathbf{PLL}} + \mathbf{G_{cvac}} \left(K\mathbf{G}^{\mathbf{v}}_{\mathbf{Q}} + \mathbf{G}^{\mathbf{v}}_{\mathbf{PLL}} \right) \\ + \mathbf{G_{cvdc}}\mathbf{G_{vdcv}} \end{matrix} \right) \end{bmatrix} \right\}^{-1} \cdot \left[\mathbf{I} + \mathbf{G_{id}}(\mathbf{T} + \mathbf{G_{ci}}\mathbf{G_{cvdc}}\mathbf{G_{vdcd}})^{-1}\mathbf{G_{ci}} \left(\mathbf{G_{cvac}} K \mathbf{G}^{\mathbf{i}}_{\mathbf{Q}} + \mathbf{T} \right) \right] \tag{5}$$

where $\mathbf{Y_{ol}}$, $\mathbf{G_{id}}$, $\mathbf{G_{vdcd}}$, and $\mathbf{G_{vdcv}}$ are the open-loop transfer functions that can be derived from the state-space averaging model presented in Appendix A; $\mathbf{T}$, $\mathbf{G_Q}^{\mathbf{v}}$, **and** $\mathbf{G_Q}^{\mathbf{i}}$ are constant matrices; $\mathbf{I}$ is the unity matrix; $\mathbf{G_{ci}}$, $\mathbf{G_{cvdc}}$, and $\mathbf{G_{cvac}}$ are the transfer function matrices for the current loop, dc voltage loop, and ac voltage loop, respectively; $\mathbf{G_{PLL}}^{\mathbf{d}}$, $\mathbf{G_{PLL}}^{\mathbf{i}}$, and $\mathbf{G_{PLL}}^{\mathbf{v}}$ represent the effects of PLL. Some of the detailed expressions can be found in Appendix B. With this impedance model, one can clearly see the effects of each control parameter and will be discussed in the following sections.

A. Effects of AC Voltage Loop

This section investigates the effects of the ac voltage loop, i.e., the term $\mathbf{G_{cvac}}$ in (5). As the ac voltage loop is at about 10 Hz, it is expected that the effects take place in this frequency range. Fig. 8 shows the impedances of STATCOM 1 $\mathbf{Z_{vsi}}(s)$ and the rest of the grid $\mathbf{Z_{grid}}(s)$, with an increasing ac voltage loop bandwidth from 7 to 16 Hz, indicated by arrows. The solid lines are the impedances of STATCOM 1 $\mathbf{Z_{vsi}}(s)$ and relatively larger in the frequency range of several hertz than the impedances of the rest of the grid $\mathbf{Z_{grid}}(s)$ indicated by dashed lines. Note that

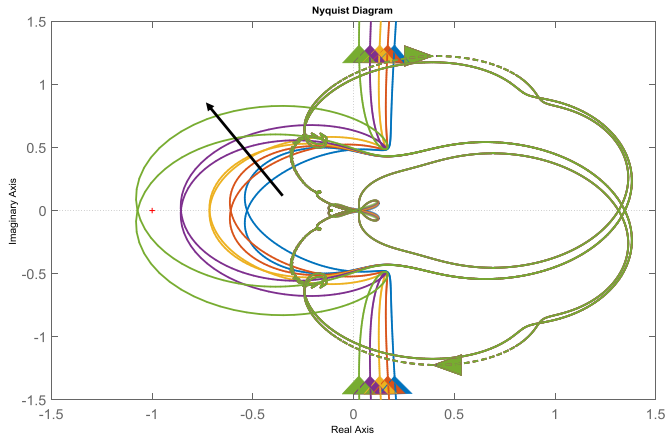

Fig. 9. Characteristic loci at STATCOM 1 terminal with respect to ac voltage loop: solid line–$\lambda 1$; dashed line—$\lambda 2$.

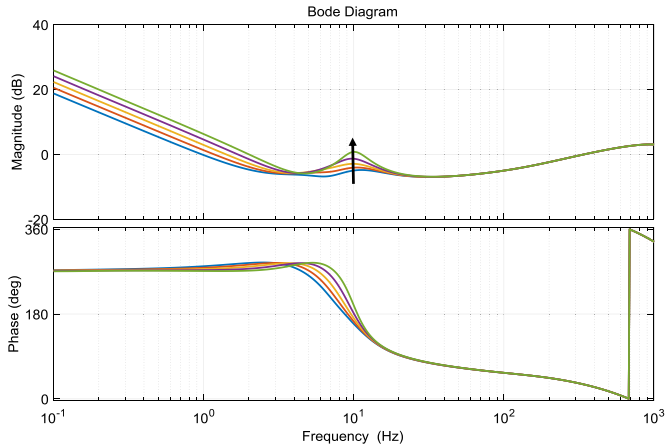

Fig. 10. Characteristic loci $\lambda 1$ at STATCOM 1 terminal with respect to ac voltage loop in the Bode plot.

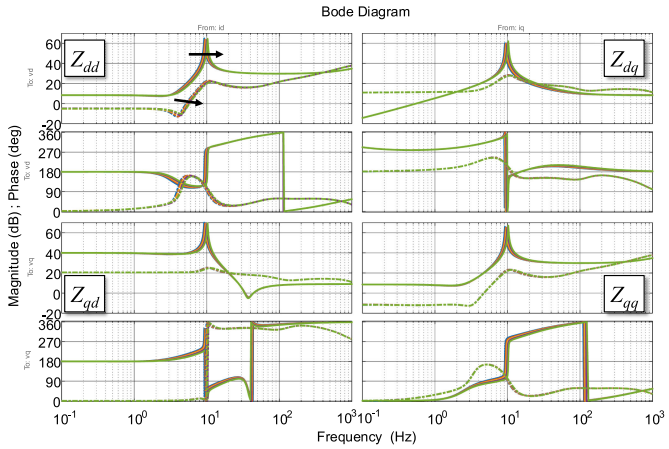

Fig. 11. Impedances at STATCOM 1 terminal with respect to PLL: solid line—$\mathrm{Z_{vsi}}$; dashed line—$\mathrm{Z_{grid}}$.

there is a resonant peak in the STATCOM impedance at about 10 Hz, and this is created by the ac voltage loop [36]. With the bandwidths increasing, the resonant peak as a result of the ac voltage loop moved to the high frequency in $\mathbf{Z_{vsi}}(s)$ and the same change happened in the impedances of the other STATCOMs due to the identical control. The grid-side impedance $\mathbf{Z_{grid}}(s)$ hence changed with the similarly moving resonant peak as well, because the impedance change of the other STATCOMs was reflected through transmission lines, which were relatively small in impedance magnitude due to close physical distance. That is to say, $\mathbf{Z_{grid}}(s)$ included the dynamic behavior of the other STATCOMs, and the STATCOMs saw small-signal impacts from each other because of short distance in between, and therefore, they could possibly interact with each other.

The eigenvalues $\lambda_1(s)$ and $\lambda_2(s)$ of the return ratio $\mathbf{L}(s) = \mathbf{Z_{grid}}(s)\mathbf{Z_{vsi}}(s)^{-1}$ were used to plot the characteristic loci in the Nyquist plot in Fig. 9, and the arrow indicates $\lambda_1(s)$ with the increase in the ac voltage loop bandwidth. One of the loci, $\lambda_1(s)$, was relatively large in magnitude, intersecting the negative real axis and the unity circle, whereas the other one, $\lambda_2(s)$, was far away from the critical point $(-1+j0)$. Neither the impedance $\mathbf{Z_{grid}}(s)$ nor the admittance $\mathbf{Y_{vsi}}(s)$ contained RHP poles because all the four STATCOMs were able to operate by themselves. As the bandwidth increased, the characteristic loci moved closer to the critical point from the origin point and eventually encircled it, indicating that the system finally fell into instability with the highest ac voltage loop bandwidth at 16 Hz, which corresponds to the simulation results presented in Section III. To this end, impedances measured at the terminal of STATCOM 1 have predicted the system stability but the reason behind is yet to be explored.

To pinpoint the reason of possible instability, Fig. 10 plots the eigenvalues $\lambda_1(s)$ from Fig. 9 in the Bode plot. When the characteristic loci reach 180° in the Bode plot, they cross the negative real axis in the Nyquist plot; if at this frequency the magnitude is greater than 0 dB, then they intersect the negative real axis outside the unity circle. According to the low- and high-frequency behaviors, this means encirclements of the critical point, because the magnitude of the locus increased and then decreased around the intersection frequency. With the increased bandwidth of the ac voltage loop, a resonant peak in the eigenvalues $\lambda_1(s)$ showed up because of the change in the impedance of both $\mathbf{Z_{vsi}}(s)$ and $\mathbf{Z_{grid}}(s)$. For the highest ac voltage loop bandwidth, the magnitude was larger than 0 dB when it intersected with the negative real axis, causing encirclements and thus instability. Although the impedances alone indicated nothing about reasons of instability, the characteristic loci in the Bode plot showed that the resonant peak from the ac voltage loop caused the instability. One can conclude that the increment of the ac voltage loop enlarged the impedance of STATCOMs, especially the resonant peak around the oscillatory frequency, which reflected to the terminal of the other STATCOMs and finally escalated the possibility that STATCOMs could interact with each other. This clearly showed how the ac voltage loop control influenced the small-signal stability, from the *d*–*q* frame impedance point of view.

B. *Effects of PLL*

The effects of PLL on impedances are plotted in Fig. 11 with increasing bandwidth from 5 to 10 Hz. Similarly, the solid lines

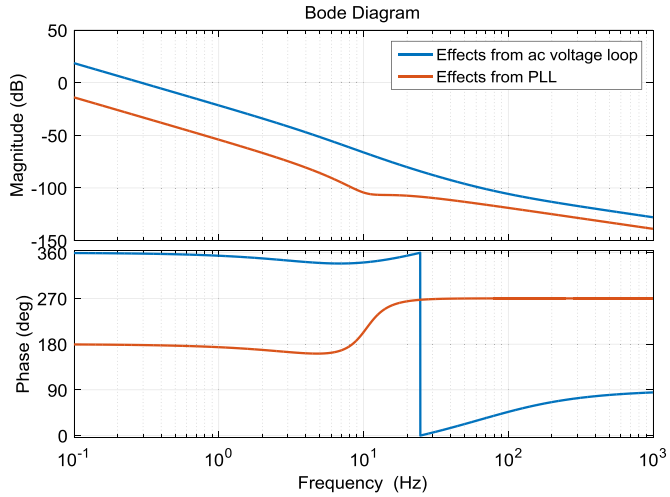

Fig. 12. Comparison of PLL and ac voltage loop effects on impedances.

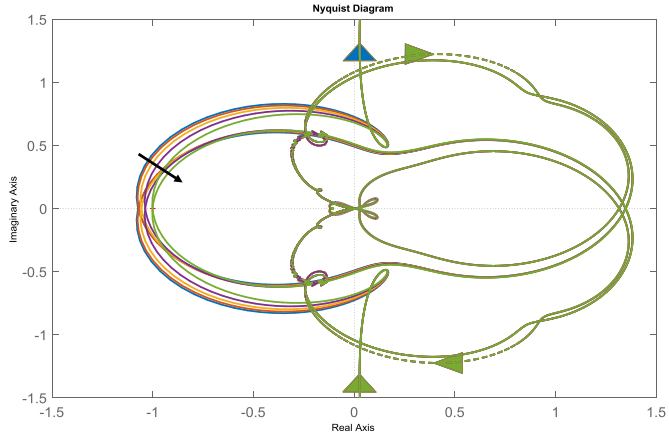

Fig. 13. Characteristic loci at STATCOM 1 terminal with respect to PLL: solid line—λ1; dashed line—λ2.

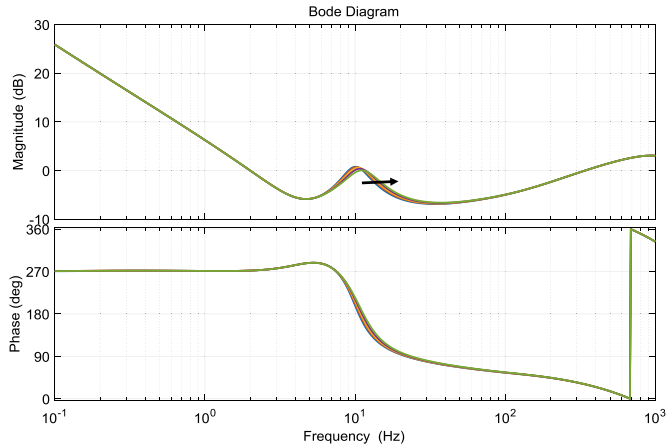

Fig. 14. Characteristic loci λ1 at STATCOM 1 terminal with respect to PLL in the Bode plot.

are the impedances of STATCOM 1 $\mathbf{Z_{vsi}}(s)$ and relatively larger in the frequency range of several hertz than the impedances of the rest of the grid $\mathbf{Z_{grid}}(s)$ shown by dashed lines. Still, the increase in bandwidth resulted in the resonant peak moving to high frequency in both $\mathbf{Z_{vsi}}(s)$ and $\mathbf{Z_{grid}}(s)$ for the same reason as in Section IV-A. However, compared with the ac voltage loop, PLL showed smaller impacts on impedances, implying that the found instability was more dependent on ac voltage loop instead of PLL.

That is to say, the origin of this instability was mostly ac voltage regulation instead of synchronization. It can be further confirmed if we take a look at how these two loops affected STATCOM impedances, with details and derivations in [11] and [36], with the approximations of those two, respectively

$$\text{AC voltage loop}: \left(k_{pi}+\frac{k_{ii}}{s}\right)\left(k_{pvac}+\frac{k_{ivac}}{s}\right) \tag{6}$$

$$\text{PLL}: \left[D_d^s-\left(k_{pi}+\frac{k_{ii}}{s}\right)\left(k_{pvac}+\frac{k_{ivac}}{s}\right)V_{\text{PCC}q}^s\right] \cdot \frac{k_{p\text{PLL}}+\frac{k_{i\text{PLL}}}{s}}{s+V_{\text{PCC}d}^s\left(k_{p\text{PLL}}+\frac{k_{i\text{PLL}}}{s}\right)}. \tag{7}$$

From Fig. 12, it is clear that the effects on STATCOM impedances from the ac voltage loop in (6) is much larger than those from PLL in (7), which shows that the PLL effects are masked by those of the ac voltage loop. Although this masking effect is dependent on operating points, especially on grid voltage level and STATCOM power ratings, the conclusion still holds valid for transmission grids. Furthermore, the higher the power system voltage $V_{\text{PCC}d}$, the smaller the effects from PLL; the smaller the line inductance L_g, the larger the effects from the ac voltage loop because of the ac voltage loop controller, according to (3). For the parameters used in simulation, the effects from ac voltage loop are about 100 times larger than those from PLL. They would only be comparable if the grid voltage drops to ten times smaller and the grid impedance increases to ten times larger, which is unlikely to happen in a transmission grid under normal conditions. Overall, the ac voltage loop has much greater influences than PLL on STATCOM impedance and, therefore, has much more contributions to small-signal stability. Hence, the ac voltage loop is the main reason of potential instability in Section III. In weak power systems with low voltage levels, instability could be because of synchronization, as reported in [29].

The characteristic loci are drawn in from the impedances in Fig. 13. $\lambda_2(s)$ shown by in dashed lines was far away from the critical point and $\lambda_1(s)$ had potential to encircle the critical point. The arrow indicates that when the bandwidth of PLL increased, the system was inclined to be stable, as the characteristic loci approached to the unity circle from the outside and did not encircle the critical point in the end with no RHP poles in either $\mathbf{Z_{grid}}(s)$ or $\mathbf{Y_{vsi}}(s)$. One can also observe that the change in charateristic loci with different bandwidths of PLL was relatively small, as explained above. This corresponds to the simulation results shown in the previous section.

Again, the first eigenvalue $\lambda_1(s)$ is plotted in the Bode plot in Fig. 14. The increase in the bandwidth of PLL did not cause a rise of resonance but moved the peak to high frequency.

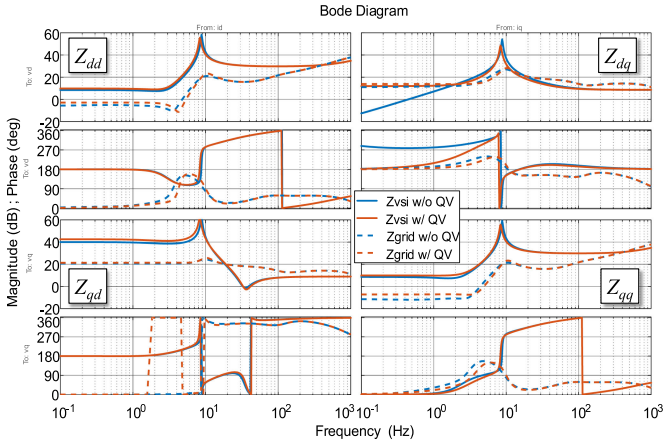

Fig. 15. Impedances at STATCOM 1 terminal with respect to QV droop: solid line—Z_{vsi}; dashed line—Z_{grid}.

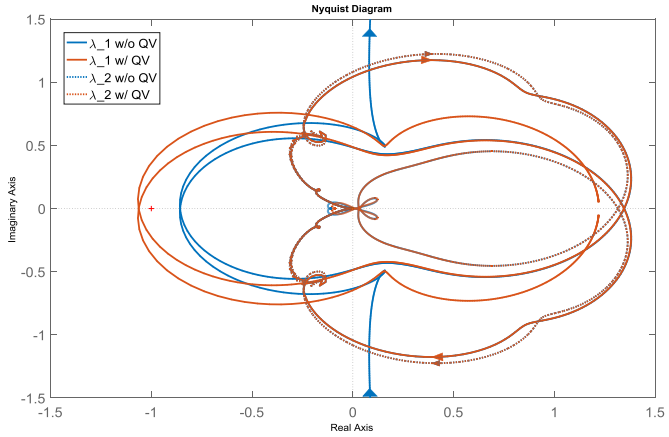

Fig. 16. Characteristic loci at STATCOM 1 terminal with respect to QV droop: solid line—λ1; dashed line—λ2.

This actually made the characteristic locus intersect with the negative real axis at a higher frequency where its magnitude was smaller. When the magnitude was smaller than 0 dB at the intersection frequency, the locus did not encircle the critical point, indicating a stable operation.

C. *Effects of QV Droop*

As for the QV droop, the impedances of STATCOM 1 and the rest of the grid were measured and shown in Fig. 15, where the solid lines represents STATCOM impedance $\mathbf{Z_{vsi}}(s)$, and the dashed lines represents $\mathbf{Z_{grid}}(s)$. The case with QV droop in red lines had one significant difference compared with the case without QV droop in blue lines: The STATCOM impedance in d–qchannel was much larger at low frequencies. This is because the reactive power is mainly dependent on q-channel current and the d-channel PCC voltage is the controlled variable of the QV droop. By activating the droop, q-channel current has equivalently more influence on the d-channel PCC voltage, which indicates larger impedance in the d–q channel. The ac voltage regulation mode without the QV droop in Section IV-A can be considered as a special case where the droop coefficient $K = 0$. As K increases, the QV droop introduced more interactions among STATCOM units in the steady state by the means of adding one feedback loop to the ac voltage loop. From (5) and (16), K affects the ac voltage controller $\mathbf{G_{cvac}}$ by adding constants that are related to the operating point. The addition not only changed the operating points but the dynamics of the ac voltage loop as well.

The characteristic loci are drawn in Fig. 16 and are calculated from the impedances presented in Fig. 15. The case with QV droop is plotted in red, and the case without QV droop is depicted in blue. Similarly, $\lambda_2(s)$, shown by dashed line, were far way from the critical point and $\lambda_1(s)$ shown by solid lines were close. Because of the addition feedback loop from the QV droop, characteristic locus $\lambda_1(s)$ with QV droop encircled the critical point and indicated instability, which matches the simulation results in the previous section.

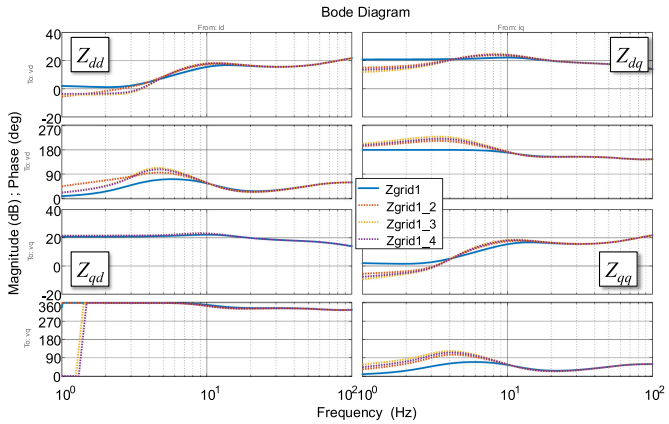

Fig. 17. Grid impedance with different STATCOMs.

D. *Effects of STATCOM Location*

Different locations of STATCOMs showed negligible effects on impedances, and, therefore, trivial influences on stability. Fig. 17 depicts the grid impedance $\mathbf{Z_{grid}}(s)$ at the terminal of STATCOM 1 with no other STATCOMs $\mathbf{Z_{grid1}}(s)$ in blue solid lines, with only STATCOM 2 $\mathbf{Z_{grid1\_2}}(s)$ in red-dashed lines, with only STATCOM 3 $\mathbf{Z_{grid1\_3}}(s)$ in yellow-dashed lines, and with only STATCOM 4 $\mathbf{Z_{grid1\_4}}(s)$ in purple-dashed lines connected respectively. $\mathbf{Z_{grid1}}(s)$ shows the equivalent impedance of the grid network and loads while the other three contained impedances from other STATCOMs, respectively. No matter which STATCOM was connected, except STATCOM 1, the grid impedances $\mathbf{Z_{grid1\_2}}(s)$, $\mathbf{Z_{grid1\_3}}(s)$, and $\mathbf{Z_{grid1\_4}}(s)$ were almost identical with less than 1 dB differences, especially around the oscillatory frequency of 10 Hz. This is because at the oscillatory frequency, the STATCOM impedance had much larger magnitude (40–50 dB) than the equivalent impedances of all lines (less than 20 dB), which is roughly less than 0.01 H for equivalent line impedances in total. Thus, the impedance of one STATCOM played a much important role in the grid impedance at the terminal of the other STATCOMs, and the line in between was negligible. If the operating point and the control parameters

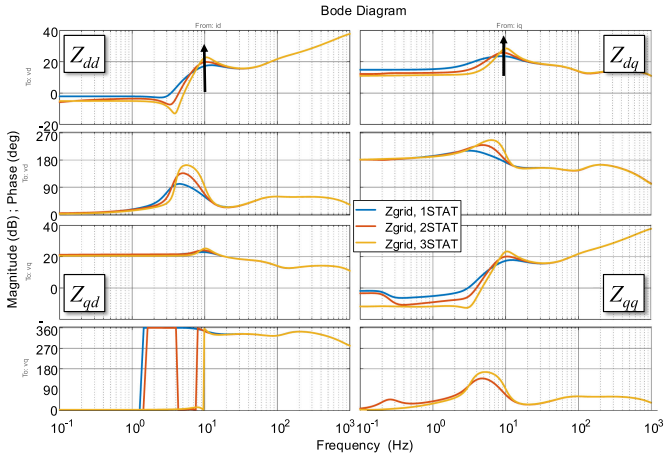

Fig. 18. Grid impedance with different numbers of STATCOMs.

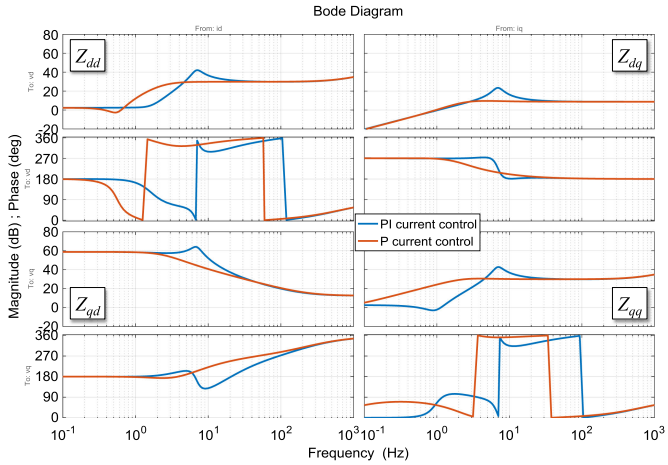

Fig. 19. STATCOM impedance with P and PI controllers for current loop.

of a specific STATCOM—STATCOM 1 in this case—did not change, the system stability was solely dependent on the grid impedance that reflects any dynamic behaviors from others. However, it was just shown that the grid impedance was little dependent on which STATCOM was connected. It leads to the conclusions that the locations of STATOMs did not matter much in the found instability with the oscillatory frequency of about 10 Hz, as well as the network topology.

One more step leads to the second conclusion that the found stability highly depended on the number of connected STATCOMs. This is shown in Fig. 18, where the grid impedance at the terminal of STATCOM with one, two, and three STATCOMs are plotted in blue, red, and yellow, respectively. The arrow indicates the increase in the number of the connected STATCOMs. It is clear that one more STATCOM made the magnitude of the resonant peak increase significantly, because all the STATCOM impedance had the same peak at the same frequency, and they added up to the grid impedance, whereas the line and load impedances were small and negligible. As discussed previously, the rising magnitude of this resonant peak tended to cause instability. Thus, the more STATCOM connected, the more unstable the system was. The number of the connected STATCOM was the main contributor to instability.

With the aforementioned conclusions, we can further infer that the combination of different STATCOMs did not influence the stability for a given number of connected STATCOMs. This answers why the connection sequence of STATCOMs did not matter in terms of stability in simulation in Section II.

V. Possible Solutions and Limitations

As discussed before, the instability between STATCOMs is due to the resonant peak in the impedance. According to Li *et al.* [36], the resonant peak in the STATCOM impedance is caused by the current loop, more specifically the integrator in the current compensator. If the integrator is removed, there will be no large impedance at the frequency of the ac voltage loop bandwidth and the resonant peak will be greatly damped. Fig. 19 shows the impedances of STATCOM with a proportional control in the current loop plotted in blue, in comparison with the proportional integral (PI) control plotted in red. The resonant peak almost disappeared and left the sections in low and high frequencies stay the same. However, without the integrator in the current controller, the regulation capability of currents within the current loop bandwidth was weakened, as the closed-loop loop gains of the current loop were much smaller than unity, meaning that the currents could not follow their references well, especially for low-frequency disturbances. In the low frequencies, the integrator in the PI controller increased the magnitude of the open-loop transfer function from the current references to the actual values, such that the controlled current could resist perturbations and track the corresponding references accurately. Without the integrator, the only regulation of currents fell into indirect control by the outer voltage loops, which is not preferable to handle complex grid conditions. Especially, the overshoot or undershoot of the current to grid transients may be very large without the integral term.

Another way to tune the STATCOM impedance is to change the ac voltage loop controller. Because a sharp resonant peak usually indicates insufficient damping and a small phase margin, alternative controllers can replace the PI controller in order to boost the phase margin to provide additional damping. STATCOM impedance was changed accordingly, as shown in Fig. 20, where the colors blue, red, and yellow show 40°, 86°, and 135° phase margins. The PI controller could achieve an 86° phase margin, which was used for evaluation previously, depicted in red and marked as "PM 86." A type II controller was designed in order to place a zero before the bandwidth to boost the phase and get a 135° phase margin, drawn in yellow and marked as "PM 135." Another controller was designed representing a low-pass filter below the bandwidth and a high-frequency zero, decreasing the phase margin to 40°, depicted in blue and marked as "PM 40." Without an additional zero before the bandwidth, the highest phase margin was only a little bit less than 90°. The lower the frequency of the additional zero before the bandwidth, the more the phase margin for the open-loop gain, and the more the damping for the resonant peak, indicating smaller possibility to interact with the other STATCOMs. However, the additional

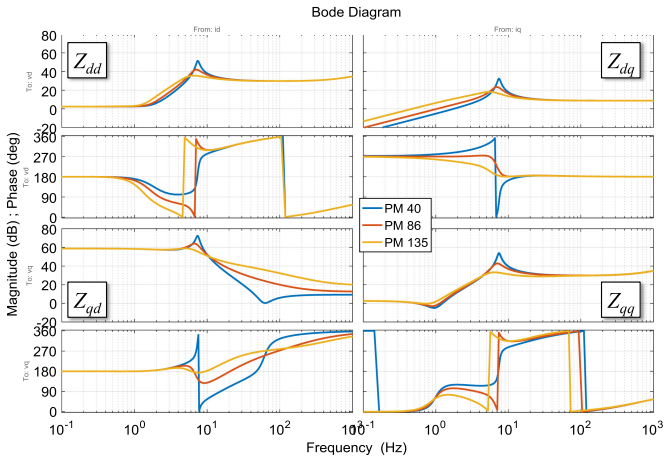

Fig. 20. STATCOM impedance with different controllers for ac voltage loop with 40°, 86°, and 135° phase margins.

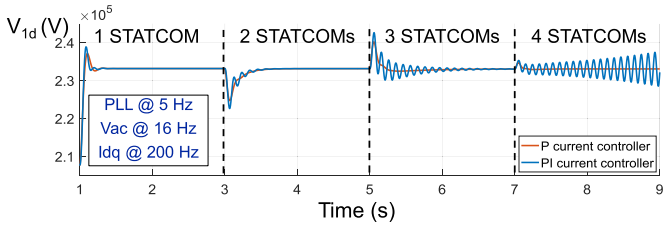

Fig. 21. Instability mitigation by a proportional current controller.

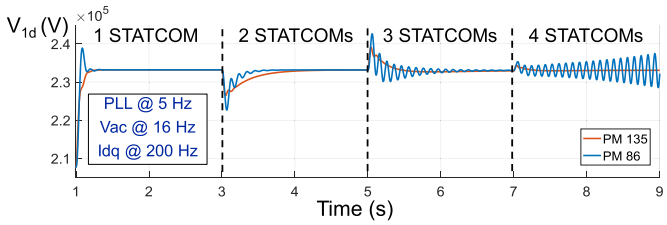

Fig. 22. Instability mitigation by alternative ac voltage controller with larger phase margin.

zero also slowed down the settling time, because the transient responses were mainly dependent on the zero with the lowest frequency.

Figs. 21 and 22 show that the above-mentioned two alternative controls could help stabilize the system. However, these two alternative controls cannot solve the instability problem fundamentally, and in other words, the problem will appear again if the ac voltage loop bandwidth is to be pushed higher. This is because the onset of the instability cannot be eliminated as the interactions between the STATCOMs always exist as long as they are in close proximity. It will be demonstrated experimentally too in the following section.

VI. Experimental Verification

Due to laboratory limitations, a scaled-down and simplified 2-STATCOM system was constructed. Two 2-level 3-phase voltage-source converters working as STATCOMs were built, one using Si-based insulated-gate bipolar transistor module PM50CL1A060 from Mitsubishi and the other using SiC-based MOSFET module CAS120M12BM2 from Cree. In order to filter out the harmonics from the switching behaviors, an *LCL* filter was implemented instead of an *L* filter. The resonant frequency of the *LCL* filter is about 1.7 kHz, which is much higher than the fastest current bandwidth and, thus, not affecting the stability under study. The converter systems are both controlled by DSP TMS320F28343 from Texas Instruments and CPLD LCMXO2-4000HC-4TG144C from Lattice integrated into one motherboard with sensing, protection, and self-startup capabilities. The gate driver boards were separately designed in order to achieve better switching performances. The parameters of passive components of both STATCOMs were chosen to be the same, as well as the control parameters, listed in Table II. The design of the STATCOM control parameters was the same as in the previous sections. STATCOMs are fully functional converter systems, including all passive components, digital control systems, and auxiliary components. With the two STATCOMs working, Fig. 23 shows the schematics of the scaled-down 2-STATCOM system, and Fig. 24 shows the picture of it. A voltage source 390-G from Pacific Power Source was used as the voltage source and resistive loads were selected with inductive line impedances in between. The two STATCOMs were regulating their own bus voltages.

TABLE II
Parameters of the Scaled-Down STATCOMs

Parameter	Symbol	Value
DC bus voltage	V_{dc}	300 V
D-channel PCC bus voltage in system d-q frame	V^s_{PCCd}	126.4 V
Q-channel PCC bus voltage in system d-q frame	V^s_{PCCq}	-15.03 V
D-channel grid side current in system d-q frame	I^s_{2d}	-3.15 A
Q-channel grid side current in system d-q frame	I^s_{2q}	-17 A
D-channel inverter side current in system d-q frame	I^s_{1d}	-2.92 A
Q-channel inverter side current in system d-q frame	I^s_{1q}	-15.32 A
Switching frequency of the STACOM	f_{sw}	20 kHz
Inductance of inverter side inductor of LCL filter	L_1	250 μH
Resistance of inverter side inductor of LCL filter	R_1	20 mΩ
Inductance of grid side inductor of LCL filter	L_2	250 μH
Resistance of grid side inductor of LCL filter	R_2	33 mΩ
Capacitance of capacitor of LCL filter	C	35 μF
Damping resistor in LCL filter	R_c	1Ω
Capacitance of the dc capacitor	C_{dc}	600 μF
Discharging resistor in dc side	R_{dc}	20 kΩ
Current controller $k_{pi} + k_{ii}/s$	k_{pi}	0.0055
	k_{ii}	2.75
PLL controller $k_{pPLL} + k_{iPLL}/s$	k_{pPLL}	0.549
	k_{iPLL}	5.49
AC voltage controller $k_{pac} + k_{iac}/s$	k_{pac}	0.034
	k_{iac}	334
DC voltage controller $k_{pdc} + k_{idc}/s$	k_{pdc}	0.043
	k_{idc}	0.144

A. Instability Between STATCOMs Due to Control

Two STATCOMs started up with the voltage source powering the loads, and dc bus voltages were charged to the nominal values

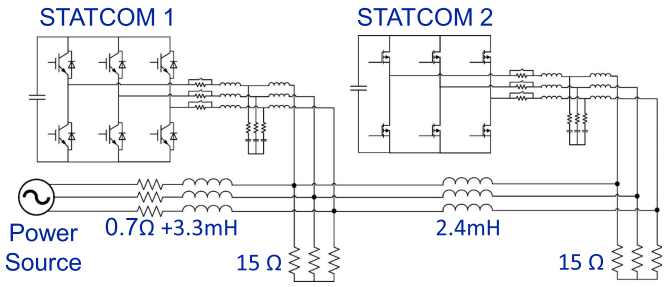

Fig. 23. Experiment circuit of two STATCOMs.

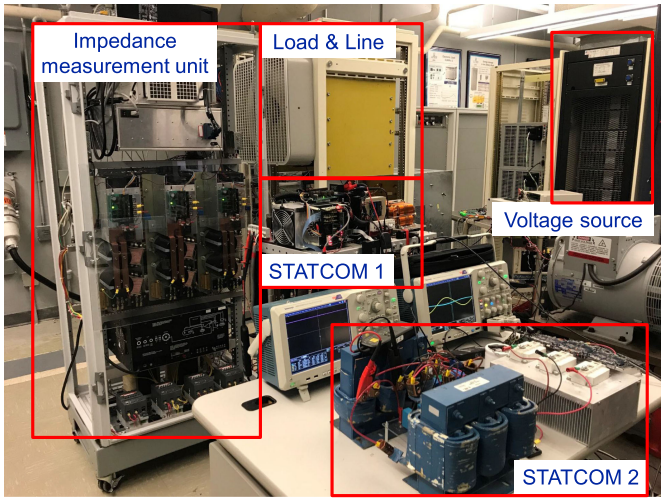

Fig. 24. Testbed for experiments.

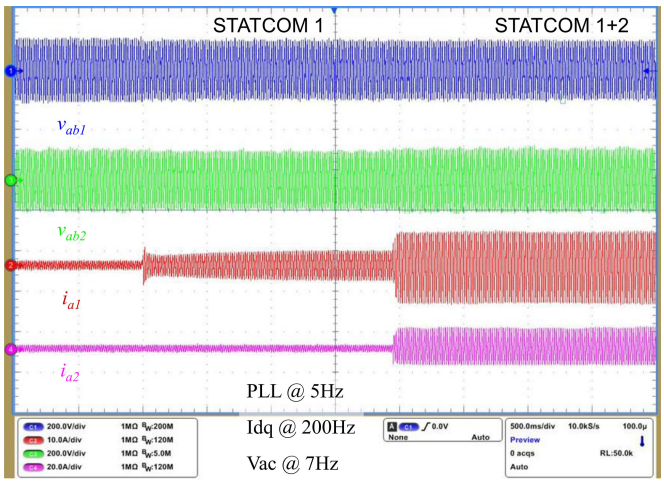

Fig. 25. Experimental waveform with two STATCOMs: a stable case.

after their controllers were synchronized with the system. Fig. 25 shows the PCC bus line-to-line voltages from phase a to phase b at the terminals of the two STATCOMs, v_{ab1} and v_{ab2}, and injecting current in phase a of the two STATCOMs i_{a1} and i_{a2} from top to bottom. At first, neither of the STATCOMs was exchanging reactive power with the grid and only a small amount of current was drawn from the grid to balance the losses in the converters. Then STATCOM 1 started to compensate reactive

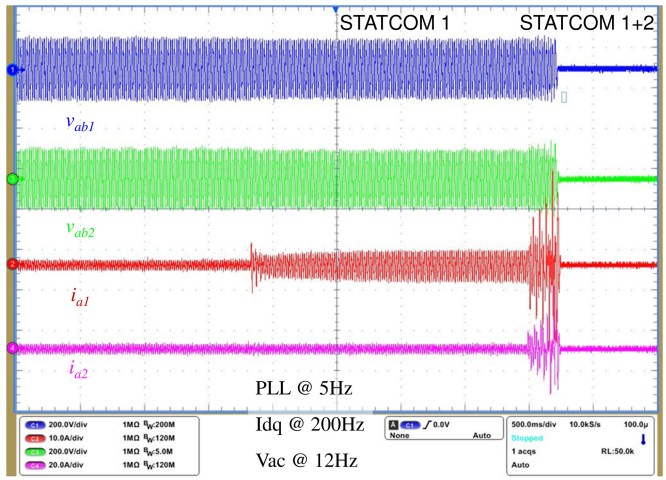

Fig. 26. Experimental waveform with two STATCOMs: an unstable case due to increased ac voltage loop bandwidth.

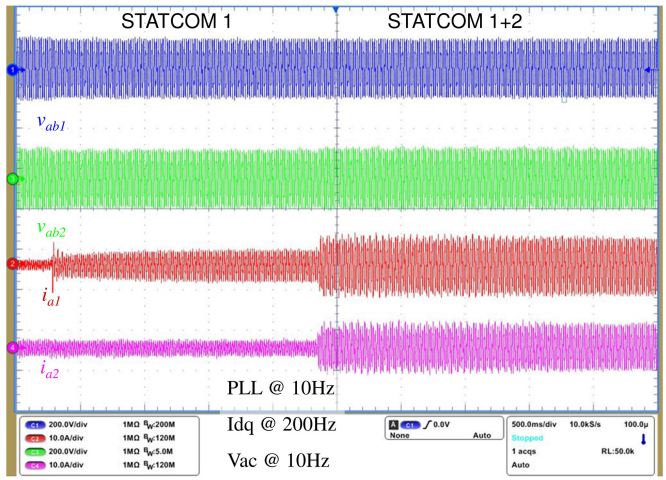

Fig. 27. Experimental waveform with two STATCOMs: a marginally stable case.

power, followed by the additional compensation of STATCOM 2, marked in Fig. 25. This case was a stable case with two STATCOMs running, where the control loop bandwidths are listed Fig. 25. If the ac voltage loop bandwidth was increased from 7 to 12 Hz, then as one can see in Fig. 26 that the system was unstable and the injecting current oscillated and, triggered the overcurrent protection in the end. The oscillatory frequency was about 102 Hz. This phenomenon verified the previous simulation that a higher ac voltage loop bandwidth tends to destabilize the system.

To find a case where the effects of PLL bandwidth were easier to observe, a marginally stable case was identified by increasing the ac voltage loop from 7 to 10 Hz and increasing the PLL bandwidth from 5 to 10 Hz, as compared with the case presented in Fig. 25. The marginally stable case is shown in Fig. 27, where the system was much less damped when STATCOM 2 began compensating reactive power. From the marginally stable case, the PLL bandwidth was reduced from 10 to 5 Hz, and the experimental results are shown in Fig. 28. The system then

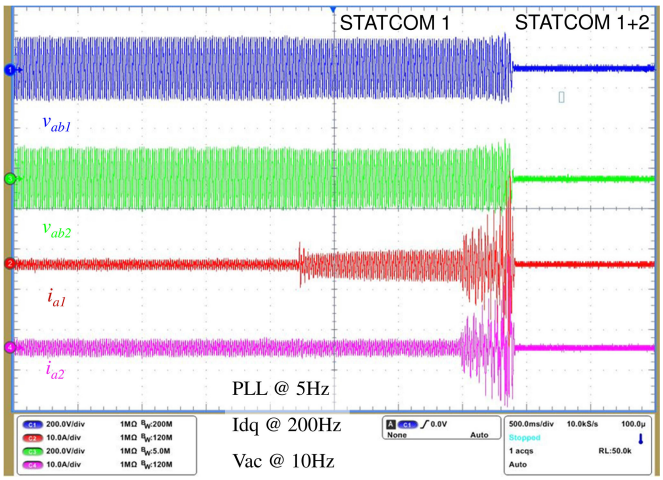

Fig. 28. Experimental waveform with two STATCOMs: an unstable case due to decreased PLL bandwidth.

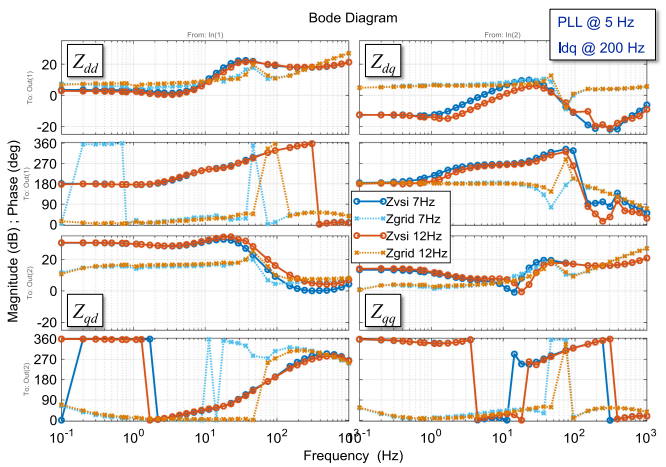

Fig. 29. Impedances at STATCOM 1 terminal with respect to ac voltage loop in experiment.

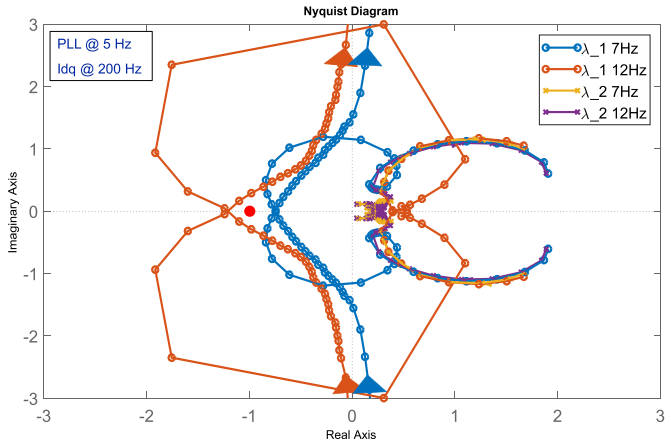

Fig. 30. Characteristic loci at STATCOM 1 terminal with respect to ac voltage loop in experiment.

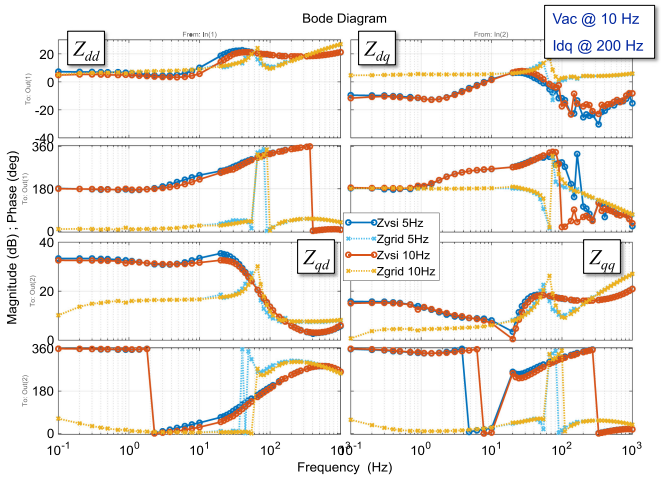

Fig. 31. Impedances at STATCOM 1 terminal with respect to PLL.

fell into instability with the overcurrent protection triggered eventually. The oscillatory frequency was about 90 Hz.

B. Impedance-Based Stability Analysis

To verify the analysis mentioned above, impedances were measured at the terminal of STATCOM 1 in the constructed scaled-down 2-STATCOM system using the impedance measurement unit (IMU) [37], as shown in Fig. 24. The IMU was inserted in series at the terminal of STATCOM 1 and was able to measure the impedances on both sides at the same time after the system reached the steady state. Using the second method mentioned in the beginning of Section IV, the impedances of both sides under two different ac voltage loop bandwidth cases (7 and 12 Hz) in the evaluation were measured and shown in Fig. 29. The impedances of STATCOM 1 are in circles, and those of the rest of the grid are in crosses. With the increasing ac voltage loop bandwidth, the resonant peak in both $\mathbf{Z}_{vsi}(s)$ and $\mathbf{Z}_{\mathbf{grid}}(s)$ moved to high frequency.

The eigenvalues in both cases were computed and plotted in Fig. 30. $\lambda_2(s)$ was always far away from the critical point, whereas $\lambda_1(s)$ encircled it when the ac voltage loop was 12 Hz. Because there was no RHP pole in either $\mathbf{Z}_{\mathbf{grid}}(s)$ or $\mathbf{Y}_{vsi}(s)$, the system was unstable at the frequency of 12 Hz. When $\lambda_1(s)$ encircled the critical point, it intersected with the negative real axis at the frequency of about 43 Hz. This oscillatory frequency was in the *d*–*q* frame and can be translated to a 103-Hz oscillation in the abc frame. In the experimental results presented in Section VI-A, the system was unstable when the ac voltage loop was 12 Hz, and the oscillatory frequency was 102 Hz, matching well with the *d*–*q* frame-based impedance stability analysis.

The impedances of $\mathbf{Z}_{\mathbf{vsi}}(s)$ and $\mathbf{Z}_{\mathbf{grid}}(s)$ were measured in the same way with respect to PLL. Two cases, 5 and 10 Hz, were evaluated. Also as discussed, the resonant peak moved with the increase in the bandwidth of PLL, which can be seen in Fig. 31. The eigenvalues in both cases were computed and plotted in Fig. 32. Similarly, $\lambda_2(s)$ was always far away from the critical point, whereas $\lambda_1(s)$ encircled it when PLL was 5 Hz. Since there was no RHP pole in either $\mathbf{Z}_{\mathbf{grid}}(s)$ or $\mathbf{Y}_{\mathbf{vsi}}(s)$, the system

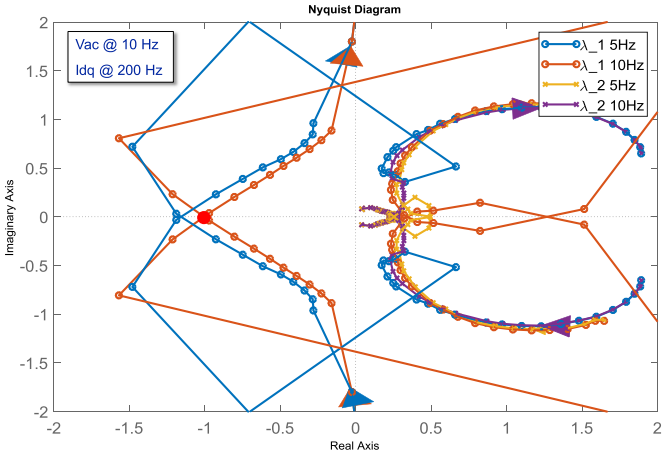

Fig. 32. Characteristic loci at STATCOM 1 terminal with respect to PLL in the experiment.

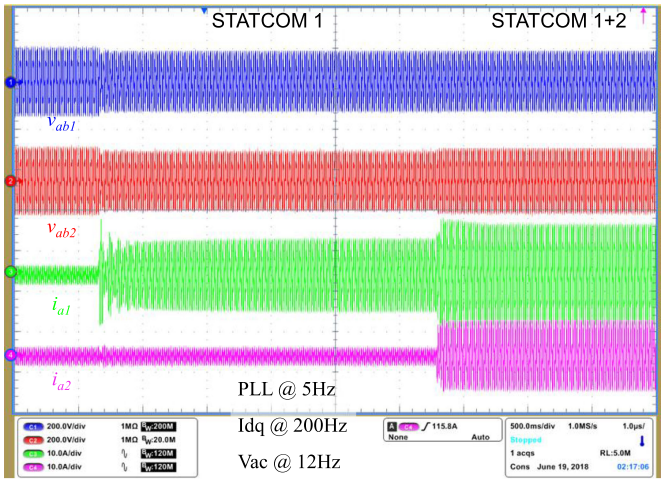

Fig. 33. Stability improvements by proportional current control in experiment.

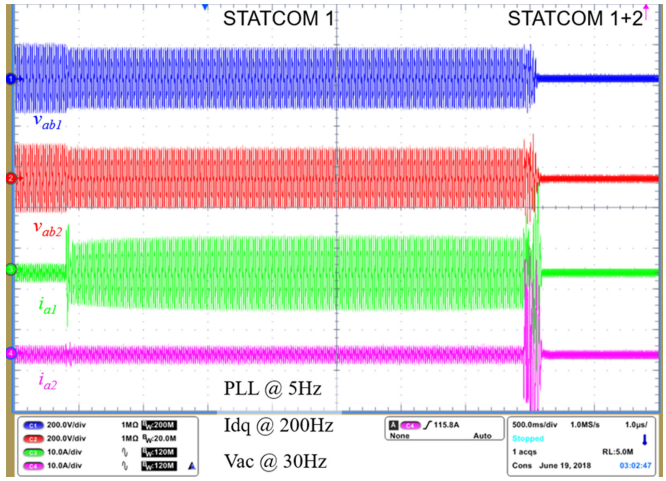

Fig. 34. Instability with increased ac voltage loop bandwidth using proportional current control.

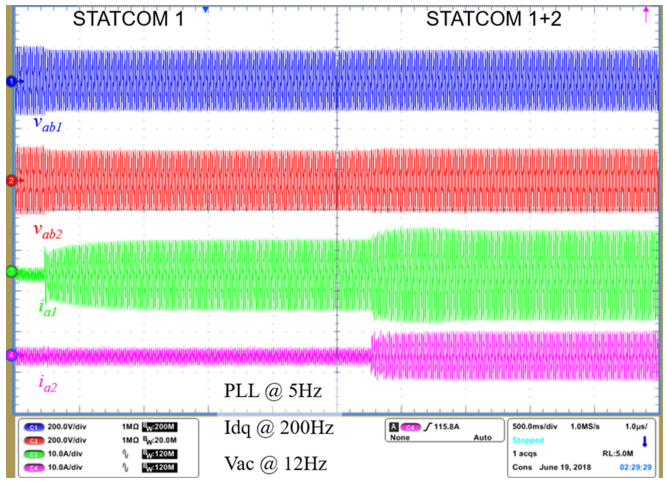

Fig. 35. Stability improvements by alternative ac voltage control in the experiment.

was unstable for the 5-Hz case. When $\lambda_1(s)$ encircled the critical point, it intersected with the negative real axis at the frequency of about 30 Hz. This oscillatory frequency was in the *d–q* frame and can be translated to a 90-Hz oscillation in the abc frame. In Section VI-A, the system was unstable when the ac voltage loop was 5 Hz and the oscillatory frequency was 90 Hz, matching well with the *d–q* frame-based impedance stability analysis.

C. Possible Solutions to Instability and Limitations

By simply removing the integral term in the current compensator and retuning the proportional term, the same bandwidth of current loop could be achieved. Fig. 33 shows the improved stability condition by the proportional current control as opposed to the unstable system presented in Fig. 26, where both cases had the same bandwidths for all control loops. Yet, a large current spike appeared when STATCOM 1 was connected and started to compensate, because its output voltage jumped due to the simple proportional term in the current loop. When the ac voltage loop bandwidth was further pushed to 30 Hz, the system would be unstable again, as shown in Fig. 34, where the current oscillated and triggered the overcurrent protection.

By moving the zero below the crossover frequency and adding one more pole after, a larger phase margin could be achieved using a type-II compensator in the ac voltage loop. Compared with the previously used PI compensator, the phase margin was increased from almost 90° to 140°. Using a type-II compensator helped the system stability, as shown in Fig. 35, whereas the system was unstable when the PI compensator for the ac voltage loop was used, as shown in Fig. 26. Although the system was stable with the type-II compensator, the settling time increased compared with the one shown in Fig. 26. This was because the zero before its bandwidth determined the time constant the most and it was at about 3 Hz, which indicated about a setting time of a second. Nonetheless, as the ac voltage loop bandwidth was further pushed to 20 Hz, the system became unstable again, as shown in Fig. 36, where the current oscillated and triggered the overcurrent protection.

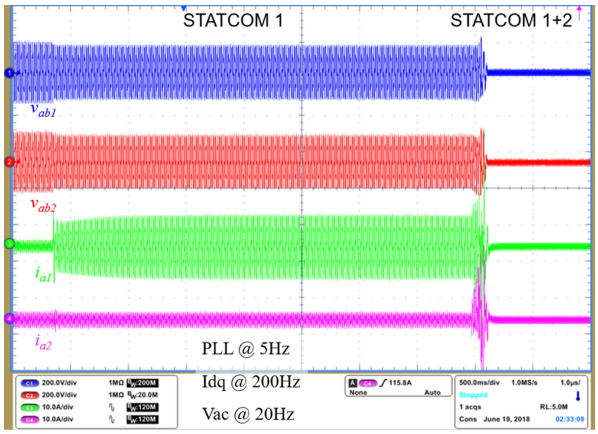

Fig. 36. Instability with increased ac voltage loop bandwidth using alternative ac voltage control.

From the above figures, it was demonstrated that both the proportional control and the type-II compensator for the ac voltage loop could improve the stability conditions, but failed when the ac voltage loop bandwidth was pushed higher.

VII. Conclusion

In this paper, potential instability in power systems with multiple STATCOMs in proximity was found due to the design of STATCOM controllers: the ac voltage controller, the PLL, and the QV droop controller. The *d–q* frame impedance-based stability analysis was used to explore the instability. From the analysis, the following conclusions were obtained. First, STATCOMs were seen to interact with each other through the transmission lines due to the relatively high magnitude of their impedances with respect to that of the lines. Second, the use of *d–q* frame impedances identified the frequency range of interactions. The ac voltage regulation was the main reason of instability among STATCOM control and masked the effects of PLL in transmission systems. This kind of instability adds new knowledge to three-phase ac systems besides CPL dynamics and synchronization, with the presence of STATCOMs. Although STATCOMs synchronize with the power grid, the instability is nonetheless due to ac voltage regulation. Third, due to the large impedance of STATCOMs around the frequency range of interactions, the number of connected STATCOMs was the main contributor to stability instead of the topology of the power system or the locations of the STATCOMs. The high magnitude of STATCOM impedance around oscillatory frequency range makes it the dominant reason of instability, whereas the topology of the power systems showed negligible influences. The use of alternative controllers could improve the stability conditions, as they can damp the resonant peak in the STATCOM impedance, which could cause instability. However, it cannot avoid the onset of instability. Finally, a scaled-down two-STATCOM power grid was built to verify the conclusions experimentally.

How to find parameters that help in stabilization using the impedance-based method is essential but not easy, because it is hard to correlate a specific control parameter to stable regions using simplified and straightforward relationships, as the exact parameter ranges that stabilize the system vary with the system parameters, such as line impedances, load flows, etc. This will be a future path from this paper.

Appendix

A. State-Space Averaging Modeling of STATCOMs

The state-space averaging modeling of STATCOMs and in the *d–q* domain is organized as follows [38]:

$$\frac{d\vec{i}_{dq}}{dt}=\begin{bmatrix}-\frac{R}{L} & \omega_n\\ -\omega_n & -\frac{R}{L}\end{bmatrix}\vec{i}_{dq}+\begin{bmatrix}-\frac{D_d}{L}\\ -\frac{D_q}{L}\end{bmatrix}v_{\rm dc}-\frac{V_{\rm dc}}{L}\vec{d}_{dq}+\frac{1}{L}\vec{v}_{\rm PCCdq}$$
$$\frac{dv_{\rm dc}}{dt}=\begin{bmatrix}\frac{D_d}{C_{\rm dc}} & \frac{D_q}{C_{\rm dc}}\end{bmatrix}\vec{i}_{dq}-\frac{1}{C_{\rm dc}R_{\rm dc}}v_{\rm dc}+\begin{bmatrix}\frac{I_d}{C_{\rm dc}} & \frac{I_q}{C_{\rm dc}}\end{bmatrix}\vec{d}_{dq}. \tag{8}$$

The controllers are written in the Laplace domain as follows:

$$\vec{d}_{dq}=\begin{bmatrix}k_{pi}+\frac{k_{ii}}{s} & 0\\ 0 & k_{pi}+\frac{k_{ii}}{s}\end{bmatrix}\left(\vec{i}^{\,*}_{dq}-\vec{i}_{dq}\right)+\begin{bmatrix}0 & -\omega_n L\\ \omega_n L & 0\end{bmatrix}\vec{i}_{dq}$$
$$\vec{i}^{\,*}_{dq}=\begin{bmatrix}\left(k_{pdc}+\frac{k_{idc}}{s}\right)\left(V^*_{\rm dc}-V_{\rm dc}\right)\\ \left(k_{pac}+\frac{k_{iac}}{s}\right)\left(v^*_{{\rm PCC}d}-v_{{\rm PCC}d}\right)\end{bmatrix}$$
$$\theta=\frac{1}{s}\left(k_{pPLL}+\frac{k_{iPLL}}{s}\right)v_{PCCq}. \tag{9}$$

B. Impedance Model of STATCOMs

Some key transfer functions presented in [36] are listed here for readers' reference. As the PLL provides the phase angle for the controller to do the Park transformation, its dynamics affect every state variable transformed in the d–q domain, which are system voltages $v_{\rm PCC}$, injecting current i, and duty cycles d. In that sense, it is necessary to model the impacts of the PLL on these three pairs of variables as follows:

$$\mathbf{G^v_{PLL}}=\begin{bmatrix}\cos\Theta & \sin\Theta+\left(V^s_{{\rm PCC}q}\cos\Theta-V^s_{{\rm PCC}d}\sin\Theta\right)G_{\rm PLL}\\ -\sin\Theta & \cos\Theta-\left(V^s_{{\rm PCC}d}\cos\Theta+V^s_{{\rm PCC}q}\sin\Theta\right)G_{\rm PLL}\end{bmatrix} \tag{10}$$

$$\mathbf{G^i_{PLL}}=\begin{bmatrix}0 & \left(I^s_q\cos\Theta-I^s_d\sin\Theta\right)G_{\rm PLL}\\ 0 & -\left(I^s_d\cos\Theta+I^s_q\sin\Theta\right)G_{\rm PLL}\end{bmatrix} \tag{11}$$

$$\mathbf{G^d_{PLL}}=\begin{bmatrix}0 & -\left(D^s_q\cos\Theta+D^s_d\sin\Theta\right)G_{\rm PLL}\\ 0 & \left(D^s_d\cos\Theta-D^s_q\sin\Theta\right)G_{\rm PLL}\end{bmatrix} \tag{12}$$

where

$$G_{\rm PLL}=\frac{k_{p\rm PLL}+\frac{k_{i\rm PLL}}{s}}{s+V^s_{{\rm PCC}d}\left(k_{p\rm PLL}+\frac{k_{i\rm PLL}}{s}\right)} \tag{13}$$

and Θ is the steady-state phase difference between the PCC voltage $v_{\rm PCC}$ and the reference voltage for the power system. The controllers are also written in their matrix form

$$\mathbf{G_{ci}} = \begin{bmatrix} k_{pi} + \frac{k_{ii}}{s} & 0 \\ 0 & k_{pi} + \frac{k_{ii}}{s} \end{bmatrix} \tag{14}$$

$$\mathbf{G_{cvac}} = \begin{bmatrix} 0 & 0 \\ k_{pac} + \frac{k_{iac}}{s} & 0 \end{bmatrix}, \mathbf{G_{cvdc}} = \begin{bmatrix} k_{\rm pdc} + \frac{k_{\rm idc}}{s} \\ 0 \end{bmatrix} \tag{15}$$

$$\mathbf{G_Q^v} = \begin{bmatrix} I_q^s & -I_d^s \\ 0 & 0 \end{bmatrix}, \mathbf{G_Q^i} = \begin{bmatrix} -V_{{\rm PCC}q}^s & V_{{\rm PCC}d}^s \\ 0 & 0 \end{bmatrix}. \tag{16}$$

The open-loop transfer functions $\mathbf{Y_{ol}}, \mathbf{G_{id}}, \mathbf{G_{vdcd}}$, and $\mathbf{G_{vdcv}}$ can be derived from (8), as defined below. Their detailed expressions can be found in [36]

$$\begin{bmatrix} \vec{i}_{dq} \\ v_{\rm dc} \end{bmatrix} = \begin{bmatrix} \mathbf{G_{id}} & \mathbf{Y_{ol}} \\ \mathbf{G_{vdcd}} & \mathbf{G_{vdcv}} \end{bmatrix} \begin{bmatrix} \vec{d}_{dq} \\ \vec{v}_{{\rm PCC}dq} \end{bmatrix}. \tag{17}$$

REFERENCES

[1] F. Shahnia, S. Rajakaruna, and A. Ghosh, *Static Compensators (STATCOMs) in Power Systems*. Singapore: Springer, 2014.

[2] Y. H. Song and A. Johns, *Flexible AC Transmission Systems (FACTS)*. London, U.K.: Institution of Electrical Engineers, 1999.

[3] N. Mithulananthan, C. A. Canizares, J. Reeve, and G. J. Rogers, "Comparison of PSS, SVC, and STATCOM controllers for damping power system oscillations," *IEEE Trans. Power Syst.*, vol. 18, no. 2, pp. 786–792, May 2003.

[4] K. R. Padiyar and N. Prabhu, "Design and performance evaluation of subsynchronous damping controller with STATCOM," *IEEE Trans. Power Del.*, vol. 21, no. 3, pp. 1398–1405, Jul. 2006.

[5] M. S. El-Moursi, B. Bak-Jensen, and M. H. Abdel-Rahman, "Novel STATCOM controller for mitigating SSR and damping power system oscillations in a series compensated wind park," *IEEE Trans. Power Electron.*, vol. 25, no. 2, pp. 429–441, Feb. 2010.

[6] W. Hai Feng, H. Li, and H. Chen, "Coordinated secondary voltage control to eliminate voltage violations in power system contingencies," *IEEE Trans. Power Syst.*, vol. 18, no. 2, pp. 588–595, May 2003.

[7] L. A. S. Pilotto, W. F. Long, F. L. Alvarado, and A. Edris, "Determination of needed FACTS controllers that increase asset utilization of power systems," *IEEE Trans. Power Del.*, vol. 12, no. 1, pp. 364–371, Jan. 1997.

[8] CIGRÉ Workshop Group 14.29, "Coordination of Controls of Multiple FACTS/HVDC Links in the Same System," CIGRÉ, 1999. [Online]. Available: https://books.google.com/books?id=3n6xHAAACAAJ

[9] Centro de Pesquisas de Energia Eletrica (CEPEL), Electric Power Research Institute, University of Wisconsin-Madison Campus. Department of Engineering Professional Development, "Analysis of control interactions on FACTS assisted power systems," Electric Power Research Institute, Palo Alto, CA, USA, 1998. [Online]. Available: https://books.google.com/books?id = G0LeHAAACAAJ

[10] C. Li and K. Thomas, "Study and assessment of Dominion's STATCOMs," in *Grid Future Symp.*, Philadelphia, PA, USA, pp. 1–6, 2016.

[11] C. Li, R. Burgos, Y. Tang, and D. Boroyevich, "Stability analysis on D-Q frame impedances in power systems with multiple STATCOMs in proximity," in *Proc. IEEE Southern Power Electron. Conf.*, Puerto Varas, Chile, 2017, pp. 1–6.

[12] E. Ghahremani and I. Kamwa, "Optimal placement of multiple-type FACTS devices to maximize power system loadability using a generic graphical user interface," *IEEE Trans. Power Syst.*, vol. 28, no. 2, pp. 764–778, May 2013.

[13] R. Sirjani, A. Mohamed, and H. Shareef, "Optimal allocation of shunt Var compensators in power systems using a novel global harmony search algorithm," *Int. J. Elect. Power Energy Syst.*, vol. 43, no. 1, pp. 562–572, 2012.

[14] Y. Del Valle, J. C. Hernandez, G. K. Venayagamoorthy, and R. G. Harley, "Multiple STATCOM allocation and sizing using particle swarm optimization," in *Proc. IEEE PES Power Syst. Conf. Expo.*, 2006, pp. 1884–1891.

[15] A. R. Messina, M. A. Pérez, and E. Hernández, "Co-ordinated application of FACTS devices to enhance steady-state voltage stability," *Int. J. Elect. Power Energy Syst.*, vol. 25, no. 4, pp. 259–267, 2003.

[16] A. Elmitwally, M. Elsaid, and M. Elgamal, "Multi-agent-based voltage stabilization scheme considering load model effect," *Int. J. Elect. Power Energy Syst.*, vol. 55, pp. 225–237, 2014.

[17] L. B. Perera, G. Ledwich, and A. Ghosh, "Multiple distribution static synchronous compensators for distribution feeder voltage support," *IET Gener., Transm. Distrib.*, vol. 6, no. 4, pp. 285–293, 2012.

[18] H. F. Wang, "Modelling multiple FACTS devices into multi-machine power systems and applications," *Int. J. Elect. Power Energy Syst.*, vol. 25, no. 3, pp. 227–237, 2003.

[19] P. Kundur, *Power System Stability and Control*. New York, NY, USA: McGraw-Hill, 1994.

[20] J. Sun, "Small-signal methods for AC distributed power systems—A review," *IEEE Trans. Power Electron.*, vol. 24, no. 11, pp. 2545–2554, Nov. 2009.

[21] C. Woei-Luen, L. Wei-Gang, and G. Hrong-Sheng, "Design of a mode decoupling STATCOM for voltage control of wind-driven induction generator systems," *IEEE Trans. Power Del.*, vol. 25, no. 3, pp. 1758–1767, Jul. 2010.

[22] R. D. Middlebrook, "Input filter considerations in design and application of switching regulators," in *Proc. IEEE Ind. Appl. Soc. Conf.*, 1976, pp. 94–107.

[23] M. Belkhayat, "Stability criteria for AC power systems with regulated loads," Ph. D. dissertation, Purdue Univ., West Lafayette, IN, USA, 1997.

[24] L. Harnefors, M. Bongiorno, and S. Lundberg, "Input-admittance calculation and shaping for controlled voltage-source converters," *IEEE Trans. Ind. Electron.*, vol. 54, no. 6, pp. 3323–3334, Dec. 2007.

[25] S. Jian, "Impedance-based stability criterion for grid-connected inverters," *IEEE Trans. Power Electron.*, vol. 26, no. 11, pp. 3075–3078, Nov. 2011.

[26] X. Wang, F. Blaabjerg, and W. Wu, "Modeling and analysis of harmonic stability in an AC power-electronics-based power system," *IEEE Trans. Power Electron.*, vol. 29, no. 12, pp. 6421–6432, Dec. 2014.

[27] B. Wen, D. Boroyevich, R. Burgos, P. Mattavelli, and Z. Shen, "Small-Signal stability analysis of three-phase AC systems in the presence of constant power loads based on measured d-q frame impedances," *IEEE Trans. Power Electron.*, vol. 30, no. 10, pp. 5952–5963, Oct. 2015.

[28] D. Dong, B. Wen, D. Boroyevich, P. Mattavelli, and Y. Xue, "Analysis of phase-locked loop low-frequency stability in three-phase grid-connected power converters considering impedance interactions," *IEEE Trans. Ind. Electron.*, vol. 62, no. 1, pp. 310–321, Jan. 2015.

[29] B. Wen, D. Dong, D. Boroyevich, R. Burgos, P. Mattavelli, and S. Zhiyu, "Impedance-based analysis of grid-synchronization stability for three-phase paralleled converters," *IEEE Trans. Power Electron.*, vol. 31, no. 1, pp. 26–38, Jan. 2016.

[30] C. Li, R. Burgos, Y. Tang, and D. Boroyevich, "Impedance-based stability analysis of multiple STATCOMs in proximity," in *Proc. IEEE 17th Workshop Control Model. Power Electron.*, 2016, pp. 1–6.

[31] L. Harnefors, X. Wang, A. G. Yepes, and F. Blaabjerg, "Passivity-based stability assessment of grid-connected VSCs—An overview," *IEEE J. Emerg. Sel. Topics Power Electron.*, vol. 4, no. 1, pp. 116–125, Mar. 2016.

[32] D. Shu, X. Xie, H. Rao, X. Gao, Q. Jiang, and Y. Huang, "Sub- and super-synchronous interactions between STATCOMs and weak AC/DC transmissions with series compensations," *IEEE Trans. Power Electron.*, vol. 33, no. 9, pp. 7424–7437, Sep. 2018.

[33] C. Li, R. Burgos, Y. Tang, and D. Boroyevich, "Application of d-q frame impedance-based stability criterion in power systems with multiple STATCOMs in proximity," in *Proc. 43rd Annu. Conf. IEEE Ind. Electron. Soc.*, Beijing, China, 2017, pp. 126–131.

[34] A. Yazdani and R. Iravani, *Voltage-Sourced Converters in Power Systems: Modeling, Control, and Applications*. Hoboken, NJ, USA: Wiley, 2010.

[35] Z. Liu, J. Liu, W. Bao, and Y. Zhao, "Infinity-norm of impedance based stability criterion for three-phase AC distributed power systems with constant power loads," *IEEE Trans. Power Electron.*, vol. 30, no. 6, pp. 3030–3043, Jun. 2015.

[36] C. Li, R. Burgos, Y. Tang, and D. Boroyevich, "Analysis of small-signal impedance of STATCOMs in d-q frame," in *Proc. 43rd Annu. Conf. IEEE Ind. Electron. Soc.*, Beijing, China, 2017, pp. 870–875.

[37] M. Jakšić *et al.*, "Medium-voltage impedance measurement unit for assessing the system stability of electric ships," *IEEE Trans. Energy Convers.*, vol. 32, no. 2, pp. 829–841, Jun. 2017.
[38] S. Hilti, D. Borowiecki, and C. Chadors, "Small-signal modeling and control of three-phase PWM converters," in *Proc. EEE Ind. Appl. Soc. Anne. Meeting*, 1994, vol. 2, pp. 1143–1150.

Chi Li (S'14–M'18) received the B.S. degree in electrical engineering from Tsinghua University, Beijing, China, in 2012, and the M.S. and Ph.D. degrees in electrical engineering from Virginia Tech, Blacksburg, VA, USA, in 2015 and 2018, respectively.

From 2012 to 2018, he was a Research Assistant with the Center for Power Electronics Systems, Virginia Tech. In 2018, he returned to Tsinghua University, where he is currently a Postdoctoral Researcher with the Department of Electrical Engineering. His research interests include solid-state transformers and control and stability of grid-tied power electronics converters and systems.

Rolando Burgos (S'96–M'03) received the B.S. degree in electronics engineering, the Electronics Engineering Professional degree, and the M.S. and Ph.D. degrees in electrical engineering from the University of Concepción, Chile, in 1995, 1997, 1999, and 2002, respectively.

In 2002 he joined, as a Postdoctoral Fellow, the Center for Power Electronics Systems (CPES), Virginia Tech Blacksburg, VA, USA, where he became a Research Scientist in 2003 and a Research Assistant Professor in 2005. In 2009, he joined ABB Corporate Research, Raleigh, NC, USA, where he was a Scientist from 2009 to 2010 and a Principal Scientist from 2010 to 2012. In 2010, he was appointed an Adjunct Associate Professor with the Electrical and Computer Engineering Department, Future Renewable Electric Energy Delivery and Management Systems Center, North Carolina State University. In 2012, he returned to Virginia Tech as an Associate Professor in the Bradley Department of Electrical and Computer Engineering, where he is currently a Professor and a member of the CPES Executive Board. His research interests include the modeling and control of power electronics converters and systems, wide-bandgap semiconductor-based power conversion, packaging and integration, electromagnetic interference, and electromagnetic compatibility, multiphase multilevel power converters, grid power electronics systems, and stability of ac and dc power systems.

Dr. Burgos is a Member of the IEEE Power Electronics Society, where he currently serves the Chair of the Technical Committee on Power and Control Core Technologies. He also serves as an Associate Editor for THE IEEE TRANSACTIONS ON POWER ELECTRONICS and the IEEE JOURNAL OF EMERGING AND SELECTED TOPICS IN POWER ELECTRONICS. He is a member of the IEEE Industry Applications Society, the IEEE Industrial Electronics Society, and the IEEE Power and Energy Society.

Bo Wen (S'11–M'15) received the B.S. degree from Xi'an Jiaotong University, Xi'an, China, in 2006, and the M.S. and Ph.D. degrees from Virginia Tech, Blacksburg, VA, USA, in 2011 and 2014, respectively, all in electrical engineering.

From 2015 to 2016, he was a Research Associate with the Department of Engineering, Electrical Engineering Division, University of Cambridge, Cambridge, U.K., and from 2016 to 2018, a Lecturer with the School of Electrical and Electronic Engineering, the University of Manchester, Manchester, U.K. From 2018 to 2019, he was a Visiting Assistant Professor with the Center for Power Electronics Systems, Virginia Tech, where he is currently a Research Assistant Professor. His current research interests include multiphase power conversion, power electronics systems modeling, integration, and stability analysis.

Ye Tang (S'15) received the B.S. and M.S. degrees in electrical engineering from Tsinghua University, Beijing, China, in 2010 and 2012, respectively. She is currently working toward the Ph.D. degree at the Center for Power Electronics Systems, Virginia Polytechnic Institute and State University, Blacksburg, VA, USA.

She worked in the Dispatch and Operation Center of Hubei Province of State Grid of China between 2012 and 2014. Her research interests include integration of renewable energy in the power system, system stability analysis, photovoltaic inverters, and energy storage devices.

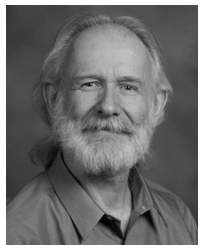

Dushan Boroyevich (S'81–M'86–SM'03–F'06–LF'18) received the Dipl.Ing. degree from the University of Belgrade in 1976 and the M.S. degree from the University of Novi Sad in 1982, in what then used to be Yugoslavia, and the Ph.D. degree from Virginia Polytechnic Institute and State University (Virginia Tech), Blacksburg, VA, USA, in 1986.

From 1986 to 1990, he was an Assistant Professor and the Director of the Power and Industrial Electronics Research Program in the Institute for Power and Electronic Engineering, University of Novi Sad. He then joined the Bradley Department of Electrical and Computer Engineering, Virginia Tech, as an Associate Professor. He is currently the University Distinguished Professor at the department and the Director of the Center for Power Electronics Systems. His research interests include electronic energy systems, multiphase power conversion, power electronics systems modeling and control, and integrated design of power converters.

Prof. Boroyevich is a member of the U.S. National Academy of Engineering. He was the President of the IEEE Power Electronics Society from 2011 to 2012. He was the recipient of numerous awards, including the IEEE William E. Newell Power Electronics Technical Field Award and the European Power Electronics Association Outstanding Achievement Award.